

Degradation analysis of GaAs solar cells at thermal stress

Nikola Papež^{a,*}, Dinara Sobola^a, Ľubomír Škvarenina^a, Pavel Škarvada^a,
Dušan Hemzal^b, Pavel Tofel^a, Lubomír Grmela^a

^a*Department of Physics, Faculty of Electrical Engineering and Communication, Brno University of Technology, Technická 2848/8, 616 00 Brno, Czech Republic*

^b*Department of Condensed Matter Physics, Faculty of Science, Masaryk University, Kotlářská 267/2, 611 37 Brno, Czech Republic*

Abstract

The work focuses on the study of structure stability and electrical parameters of photovoltaic cells based on GaAs with Ge substrate. Solar cells of this type are used especially in adverse environments such as space applications, so their working parameters should be stable even under extreme operating conditions. Changes of electrical characteristics of the cells were recorded in the form of noise measurements for examination of distinctions in the pn-junction. Current-voltage characteristics under the light illumination and in the dark environment for comparison of the cells performance were also measured. Infrared camera showed the thermal irradiation of the stressed and damaged parts and support to localize the defected areas. Atomic force microscope (AFM) was applied for observation of changes in three-dimensional topography with high resolution. Scanning electron microscope (SEM) with energy-dispersive x-ray spectroscopy (EDS) showed morphology of the solar cells and provided the elemental analysis of the samples. Raman spectroscopy provided a structural fingerprint and helped to evaluate the influence of induced degradation methods. Variations of morphology and composition were compared, detected and well-observed. Furthermore, electrical measurements proved the solar cells to be stable under temperature stresses.

*Corresponding author

Email address: Nikola.Papez@vutbr.cz (Nikola Papež)

Keywords: GaAs, solar cells, SEM, EDS, EDX, AFM, noise, infrared camera, I-V characteristics

1. Introduction

Galium arsenide (GaAs) based photovoltaic cells are generally known for their excellent properties, thanks to which they can be used under impaired conditions in demanding environments. An efficiency is closed to 30% due to their moisture resistance and UV radiation. High efficiency triple-junction GaAs solar cell is effective for applications where surface area is limited such as satellites or aircraft. They are very light due to their extreme thinness around the value at 100 μm . In most cases, thin film of GaAs is 1–2 microns thick. They also have a very low temperature coefficient which represents a smaller loss of efficiency compared to conventional silicon cells which at higher temperatures lose their efficiency much faster. Thanks to these features, GaAs cells find use for military purposes or space technologies, because this semiconductor material is mostly an expensive one. We focused on studying the properties of these cells before and after the thermal stress to verify their degradation [?].

2. Material and methods

2.1. Used and examined specimens

Several dozen samples were used and measured in this study to minimize the occurrence of random effects and errors during measurement. These are real samples that were used in the construction of Iridium satellite constellation. Each sample was cut to approximately 10×15 mm size. Measured samples are single-junction GaAs doped with aluminum (Al) and were deposited on germanium (Ge) substrate via the metalorganic chemical vapor deposition (MOCVD) process. Aluminum is often used in GaAs to expand the larger bandgap. The energy bandgap depends on the aluminum content and may vary from 1.422 to 2.16 eV. That leads to the absorption of wavelengths on the spectrum of UV light and also to increased radiation hardness. This is desirable e.g. for space

applications, for which these solar cells were specially made. The contacts are made of silver (Ag), which has also been verified by Energy Dispersive Spectroscopy (EDS). Silver is excellent conductor and contact Ag-GaAs is ohmic. In addition to common cleaning by using ultrasonic purification in isopropyl alcohol, samples did not require any further special preparation [? ? ? ?].

2.2. Thermal processing of samples

Thermal treatment was the main method of this research through which we could simulate the difficult conditions and degradation of the samples. The heat sensor was placed in close proximity to the sample, so we could monitor the exact temperature in the vicinity. The temperature was set to 350 °C. The required furnace temperature rose during 30 min. We kept it stabilized for 240 min. After that, next 30 min we waited as soon as it dropped back to room temperature of 25 °C [? ?]. All the measurements did not take place during the processing but before and after it. Processing was performed in air at normal atmospheric pressure. Slight oxidation can be expected [? ?].

2.3. Atomic force microscopy (AFM)

The AFM was used for observing the growth and shape of the newly created so-called features [?]. The microscope was preset in a semi-contact mode and a scan rate has been set to 0.4 Hz, which is equivalent to $4 \mu\text{m s}^{-1}$ [?]. This rate has been in the 10 μm scale ideal balance between image sharpness and duration measurements. The used type of microscope was NTEGRA's Prima with a NSG01 probes that had a curvature radius of the tip of 10 nm [? ?].

We also examined the S parameters. These parameters are describing the height (amplitude) of the sample. Average Roughnes is described as S_a and Root Mean Square is described as S_q . They are evaluated throughout the scanned surface, representing the total topology scale and can be used to indicate significant variations of surface condition.

The other two significant S parameters detailing the surface texture are skewness which is described as S_{sk} and kurtosis described as S_{ku} . These pa-

rameters represent a deviation from the normal distribution (i.e. bell curve). Histogram of the all measured height points describe these deviations.

The S_{sk} parameter represents the degree of symmetry of the surface height of the mean plane. If the peaks are predominant, the S_{sk} parameter grows from
60 0. But if there is a predominance of valley structures, the parameter is smaller than 0. Normally distributed surface heights has the values of $S_{sk} = 0.0$ and $S_{ku} = 3.0$.

The presence of disproportionately high peaks or depths of the valley is indicated by S_{ku} . If surfaces are not subject to extreme changes and are gradually
65 changing, they tend to have S_{ku} smaller than 3. This parameter is therefore useful for observing different surface abrasion or for observing the presence of either peak or valley defects [? ?].

2.4. Scanning Electron Microscopy (SEM) and Energy Dispersive Spectrometry (EDS)

70 Solar cells were imaged by backscattered electrons (BSE) detector on 120 μm view field at 15 kV accelerating voltage. Using EDS, we performed an elemental microanalysis of the sample at an accelerating voltage of 22 kV. By this method we analyzed the surface appearance and composition without any special preparation of the samples (cleaning or metallization). The duration of the
75 EDS analysis was 60 min. The used electron microscope was Tescan's LYRA3 with X-Max 50 EDS detector from Oxford Instruments [? ? ? ?].

2.5. Raman spectroscopy

This fast, non-destructive and very precise method was used to characterize and analyze the surface and structure of the sample. Masses of the atoms involved and strength of the bonds that were formed before and after the thermal
80 stress are important aspects. Thus, symmetry of the molecules and the individual vibrational movements strongly influences the appearance of these spectra. For observing Raman spectra Renishaw inVia tool was used. In all cases of measurement the green laser and the same laser power of 12 mW was set [? ?
85 ?].

2.6. Measurement of current-voltage characteristics

Two types of I-V characteristics were measured. The first characteristic is from the darkened chamber in reverse-bias with a limit current up to 50 mA and in forward-bias with a limit current up to 100 mA. The second was performed in an environment under illumination with a value of 1000 W m^{-2} . This characteristic was recalculated to power-voltage (P-V) curve, at which we subsequently yielded the ideal maximum working point (MPP).

During the measurement of the characteristics in the darkened chamber, the specimen was placed between two aluminum electrodes. The temperature was set at constant 25°C and was controlled by a water-cooled Peltier plate using the Keithley 2510-AT AUTOTUNING TEC sourcemeter. Keithley 2420 served as a power supply for measuring the characteristics. The results were plotted in the log-log scale.

I-V characteristics under illumination were measured using the NI PXIe-1073 measuring system with the PXI-4130 sourcemeter unit and the PXI-6224 data acquisition module. Mentioned devices are used for the measuring of electrical or physical phenomena such as voltage, current, temperature etc [?].

2.7. Noise power spectral density $S_i(f)$

Flicker noise has been the subject of several years of research where it has been shown to be closely related to the discontinuous homogeneity of a sample, such as defects, but its fundamentall origin has not been fully elucidated. This method was used for the first time to measure GaAs solar cells. Flicker noise is the type of noise known as f^{-1} , which corresponds to the inversely proportional noise power spectral density (PSD) on the frequency. This noise was measured from 10 Hz to 10 kHz range. Two aluminum electrodes in the darkened chamber between which the sample was inserted were used as the measuring apparatus. This chamber also acts as a shielding. As the supply wiring double-shielded coaxial cables were used. The circuit is closed by 5.517Ω resistor where the noise signal is detected. The specimen was powered by the Agilent E3631A

115 power supply. The noise was first amplified using the ultra-low noise preamplifier model 5184 and then wired to the R&S FMU36 baseband analyzer. The advantage of this analyzer is its high sensitivity to analyze extremely weak signals at low frequencies [?].

Noise fluctuations were measured at levels of 6, 7, 7.5, 8, 8.3, 8.6 and 9 V
120 in reverse-bias. These voltages were deliberately chosen around the knee of the specimen I-V characteristic. For comparison, it is plotted in both log-log curves with background noise, which originates from the measuring instruments [?].

2.8. Infrared camera

The surface sample before and after the thermal stress was showed using an
125 infrared camera. The picture shows a thermal difference of 0.8 °C. The type of used camera was Micro-Epsilon TIM 160 with a resolution of 160 × 120 px. The specimen was connected to the Agilent E3649A power supply and set the value of 7.3 V under reverse-biased condition, which can be seen on the darkened I-V characteristic in Figure 9 as a break point. In this way we could observe exposed
130 location on the sample. The current flowed through the sample for 3 s. After that an image was taken and then for another 3 s disconnected the sample to cool off. This process was performed 480 times and all images were averaged to eliminate the noise and other image errors [? ?].

3. Results and discussion

135 3.1. Thermal processing investigation

During the thermal processing, the treatment temperature of 350 °C was chosen as a limit value that, for a period of 240 min, the solar cells were able to withstand and continue to operate without complications. Thanks to that high temperature it is more distinctive to observe the degradation and processes
140 occurring both on the surface of the cell and its electrical properties. These processes in such a short time of thermal stress and lower temperatures may not always be measurable [?].

At this temperature a slight degradation was observed. It has been verified that if the temperature was raised up to 420 °C, nearly 90% of the measured samples were no longer functional within 30 min. The loss of their functionality has manifested itself in the form of an electrical breakdown. What type of pn-junction breakdown was going on, we continue to investigate [? ? ?].

3.2. AFM investigation

Figure 1 clearly shows the non-uniform etching GaAs. Differences are affected by the condition of the samples before processing. All of measured samples showed similar behavior. The course of degradation is thus influenced by the processing. Atomic force microscope showed with no exceptions and in all cases the more indented surface structure of the cells after processing. Differences can be seen on the non-annealed specimen in Figure 1 as compared to the annealed sample of Figure 2. These figures also show the structure in both the 2D and the 3D imaging. Such a structure may, in some cases, influence a better absorption and less reflection of light, thus gloss of the photovoltaic cell. A slight growth of features of an average height of 15.73 nm is observed after processing. That is the increase of about 5 nm compared to the non-annealed characteristics of an average height of 10.53 nm. A clear pattern of surface features is also demonstrated by the histogram in Figure 3, which confirms their growth after treatment [? ? ?].

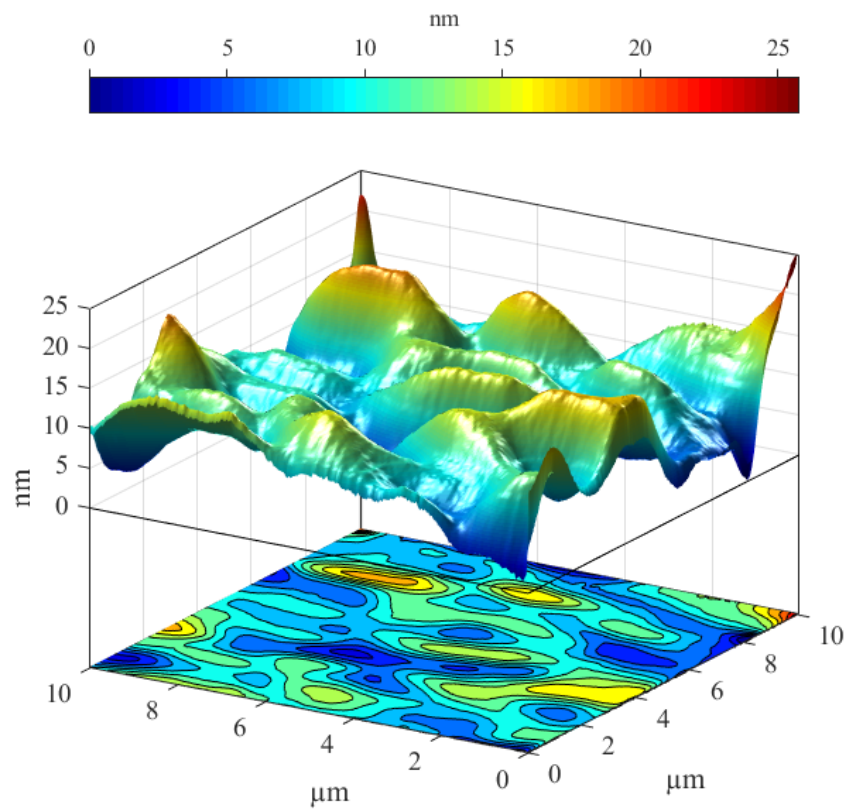


Figure 1: The surface of the solar cell before processing of dimension of $10 \times 10 \mu\text{m}$ and a height of 25 nm in 3D and 2D image created by AFM.

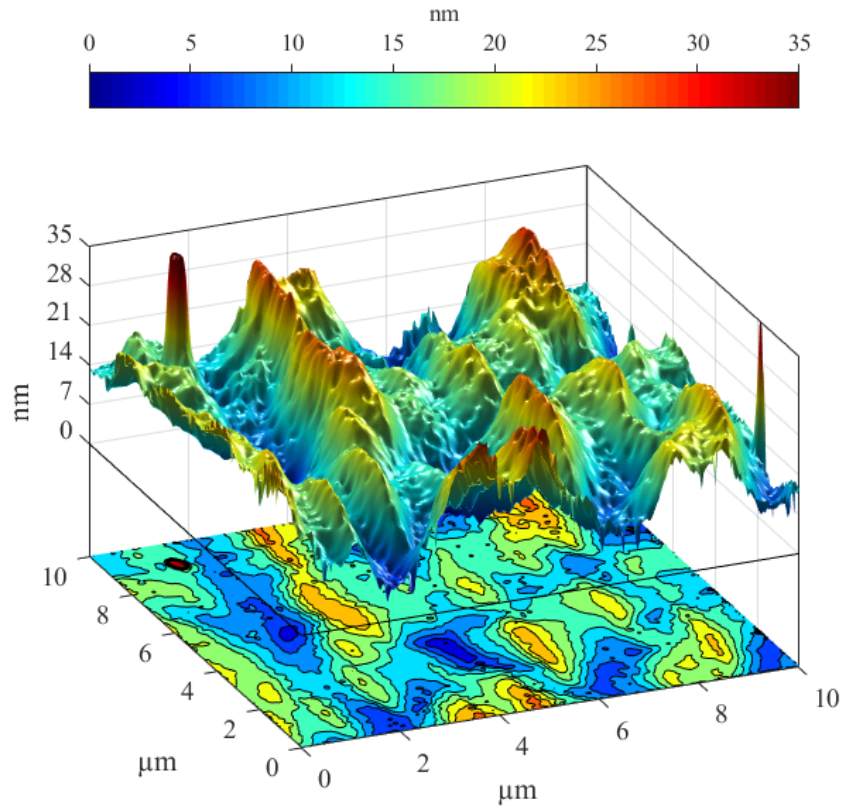


Figure 2: The surface of the cell after processing is noticeably more rugged with higher tops of features.

There were also evaluated S parameters of Average Roughness (S_a), Root Mean Square (S_q), surface skewness (S_{sk}) and coefficient of kurtosis (S_{ku}). An increase of S_a and S_q after processing can be seen from Table 1. This increase also confirms the more rugged structure, and on the contrary the decreasing parameters of S_{sk} and S_{ka} , signifying greater symmetry and surface changes.

Table 1: Surface S parameters

	S_a [nm]	S_q [nm]	S_{sk} [-]	S_{ku} [-]
Before processing	2,357	2,996	0,316	0,247
After processing	3,781	4,726	0,132	-0,227

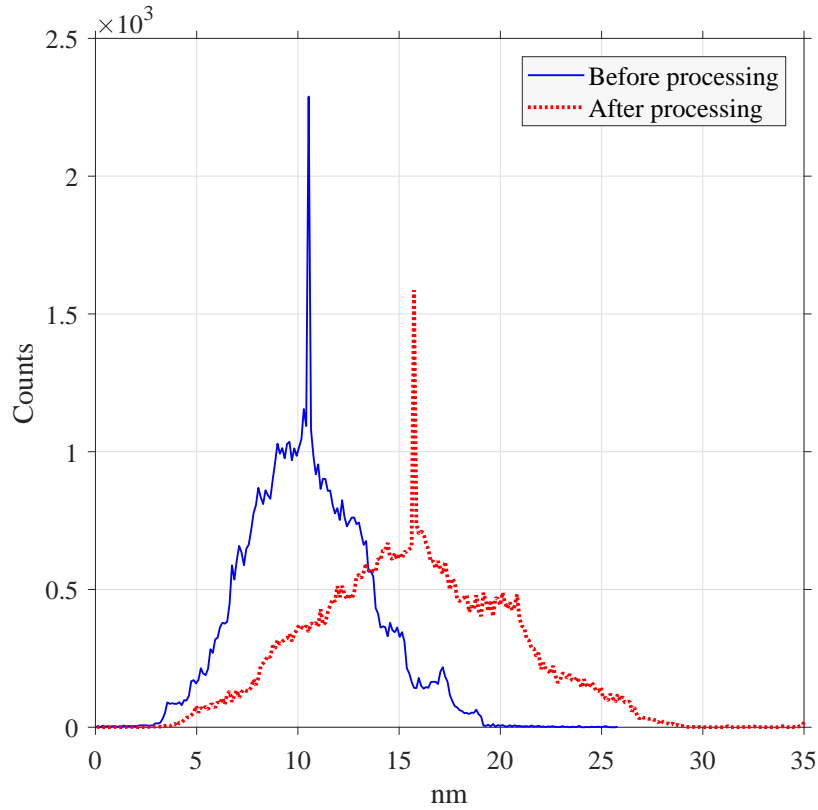


Figure 3: Histogram of occurrence of the height points of one specimen before and after the thermal processing.

3.3. SEM investigation

Surface of the sample showed less signs of degradation. The contact on the
 170 cell was kept firm after processing. Its separation was not observed and only
 moderate oxidation of the silver occurred. The differences are visible in Figure 4

and 5 [?].

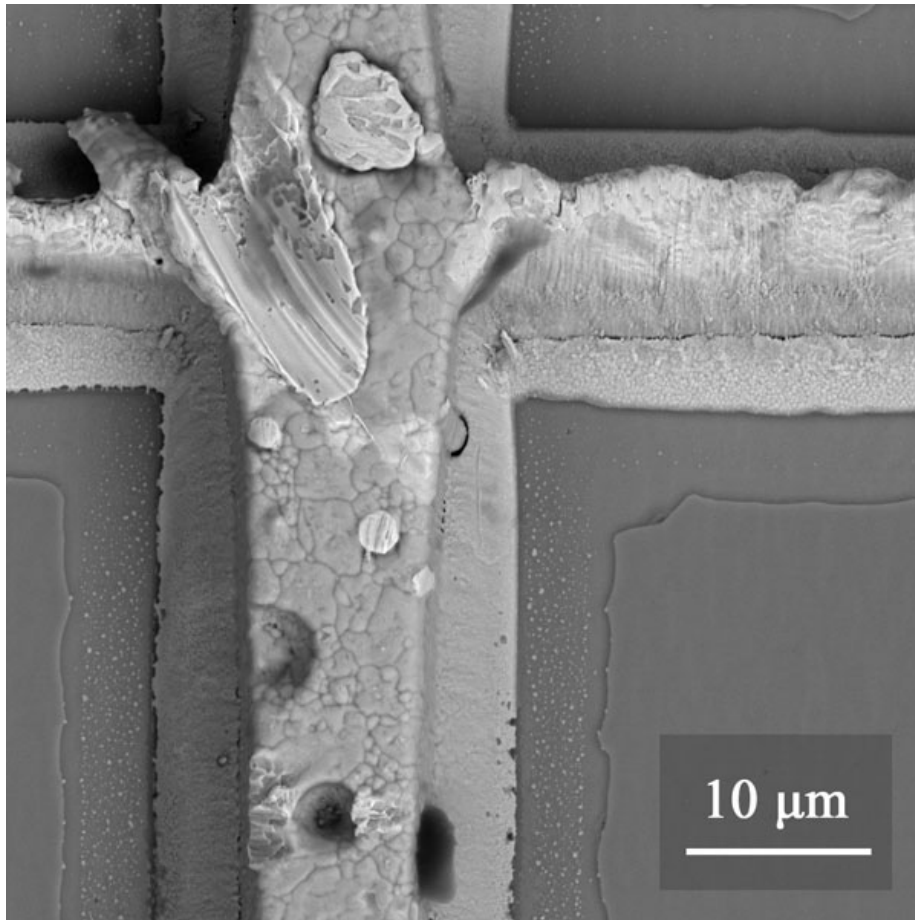


Figure 4: The contact and surface of the GaAs solar cell scanned by SEM using a BSE detector before thermal processing.

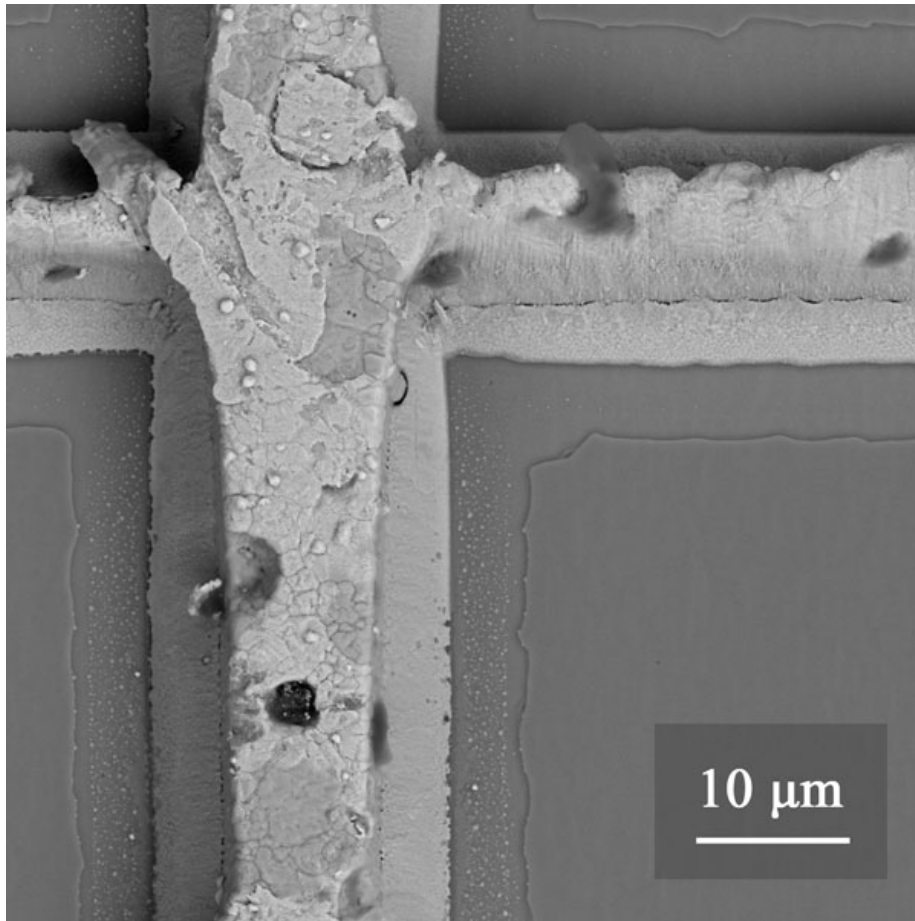


Figure 5: The GaAs solar cell exhibits slight changes in the form of oxidation on the surface of the contact after processing. Changes on the surface of the cell are not noticeable.

During the high temperature stress of the given GaAs surface the atoms of silver can diffuse into the structure of semiconductor. It is a desirable phenomenon that can improve the electrical properties of the solar cell. However, it must be reckon with the undesirable phenomena that will change some properties of the semiconductor and the conductor thermally e.g. a degree of thermal expandability [?].

3.4. Surface analysis by EDS

Surface degradation of the contact was investigated by SEM. EDS was fo-

cused only on the GaAs surface and confirms the excellent material stability. On the spectrum in Figure 6, there are almost two overlapping curves with marked elements. The weight of the individual elements and their comparison after thermal stress are also expressed as percentage. For a larger overview, changes and differences in element distribution after processing are highlighted in Figure 7. This is the subtract of EDS spectra before and after thermal stress. The difference in intensity was observed in the order of thousands of counts, which is almost negligible, as can be seen in Figure 6. Similarly, there are weight differences of the elements from the supplementary bar graph in Figure 7 [?].

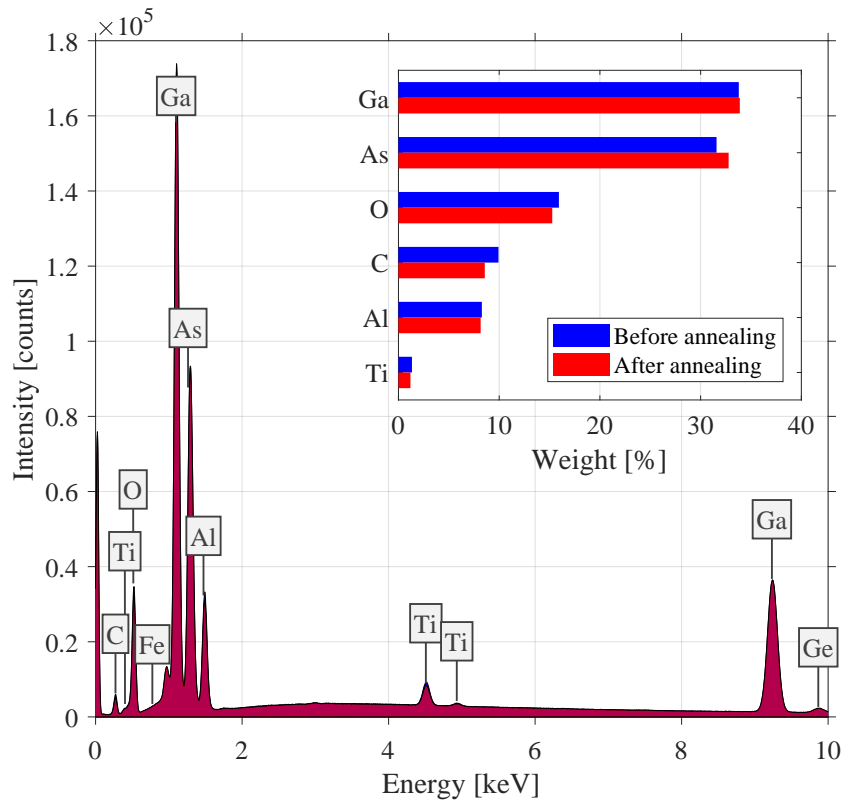


Figure 6: Energy Dispersive X-ray analysis of two identical and mutually overlapping spectra together with a percentage comparison of their weight ratio.

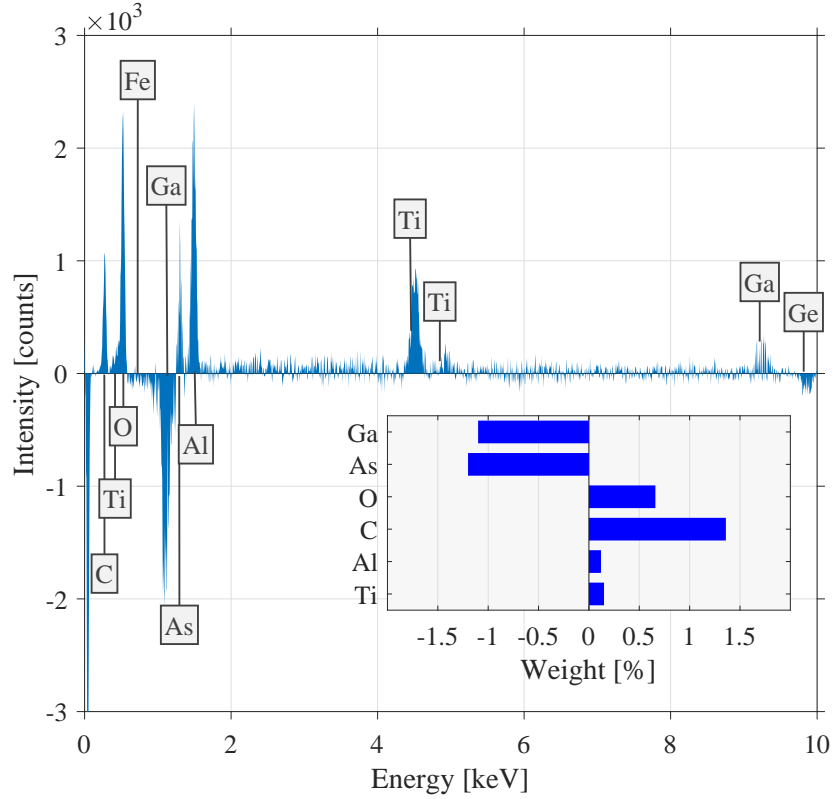


Figure 7: Difference spectrum intensity in elemental structure of the cell after thermal processing.

190 *3.5. Raman spectroscopy investigation*

For proper comparison of the two spectra before and after the treatment a reference peak has been created on the x-axis of -100 cm^{-1} . According to this peak, curves over one another was overlaid, so the differences can be correctly compared in their character. Main area of interest of experimental Raman spectrum in $55 \text{ to } 700 \text{ cm}^{-1}$ are two characteristic peaks on $268 \text{ and } 271 \text{ cm}^{-1}$. These peaks indicate the typical GaAs structure before and after thermal processing in Figure 8.

The intensity change is visible on three main peaks, which determine the amount of the proper material that has slightly decreased after processing. At

200 this point, the intensity of vibrational spectra is the least understood area of
vibrational spectroscopy. The spectrum of the sample also shows a change in
the structure of the sample. Different surface structure may be a form of varied
dislocations and the type of radiation-induced structural defects resulting from
processing. It is the purity of the material that can be observed by the frequency
205 of shift of a certain Raman line. Frequency shift between these spectra was
approximately 5 cm^{-1} , which can be considered as a relatively small change.
The full pulse width at the middle of the maximum (FWHM) expresses the
structural distribution. This is related to the life of the phonon reflected in
sharper peaks that indicate better crystalline structure of the sample. The
210 presence of defects in the sample structure will shorten phonon life and extend
the peak [? ? ?].

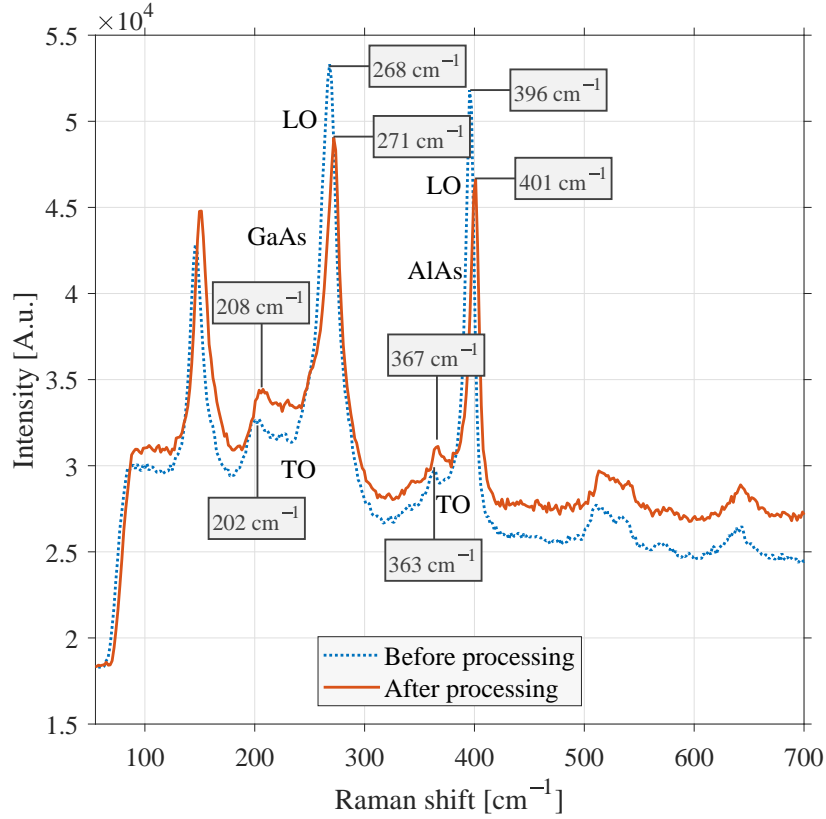


Figure 8: Raman spectrum with marked transverse-optical (TO) and longitudinal-optical (LO) bending phonon modes. The typical structure of GaAs and AlAs are also indicated.

3.6. I-V and P-V curves

At about 7 V in the reverse-bias it can be seen a electrical breakdown in the characteristic before processing in Figure 9. This significant breakdown most likely indicates a defect. There are many types of phenomena that have a similar behavior. It can be holes in the surface, dislocations, microplasma defects, mechanical damage of the surface, inhomogeneity of the sample or melted zones. It is also possible to isolate the defects in a common way using the focused ion beam, which also influences the shape of the I-V curve in reverse bias.

Break after thermal processing was not very noticeable, but the slope of the characteristic has declined. Processing temperature was so high that the

properties of the solar cell could not be fully improved, even though it was a short-term processing. There was a decrease in both, at reverse and forward biased region. That is why the deteriorating electrical properties of the cell can be confirmed, which was verified even in the case of the characteristics under illumination. A reduced short-circuit current I_{sc} was observed from 3.19 to 2.99 mA and reduced open-circuit voltage U_{oc} from 0.78 to 0.74 V in Figure 10.

The maximum working point (MPP) of the photocell determined from the power characteristic has dropped after processing. As well as the maximum power P_{max} from 1.68 to 1.11 mW and fill factor FF from 0.68 to 0.27 have decreased [?].

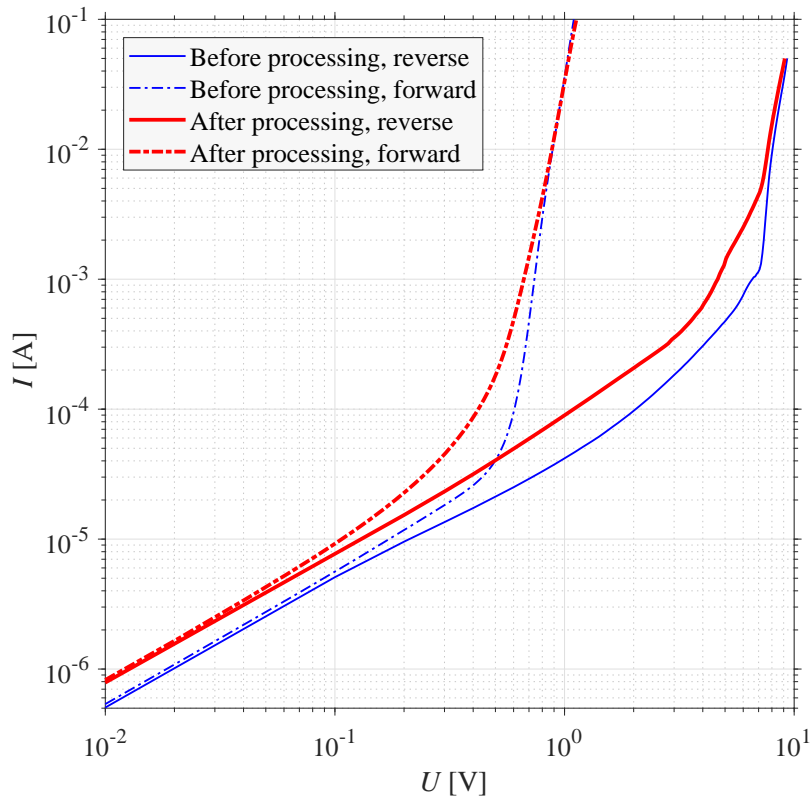


Figure 9: Current-voltage I-V curve of forward and reverse-biased solar cell before and after thermal processing.

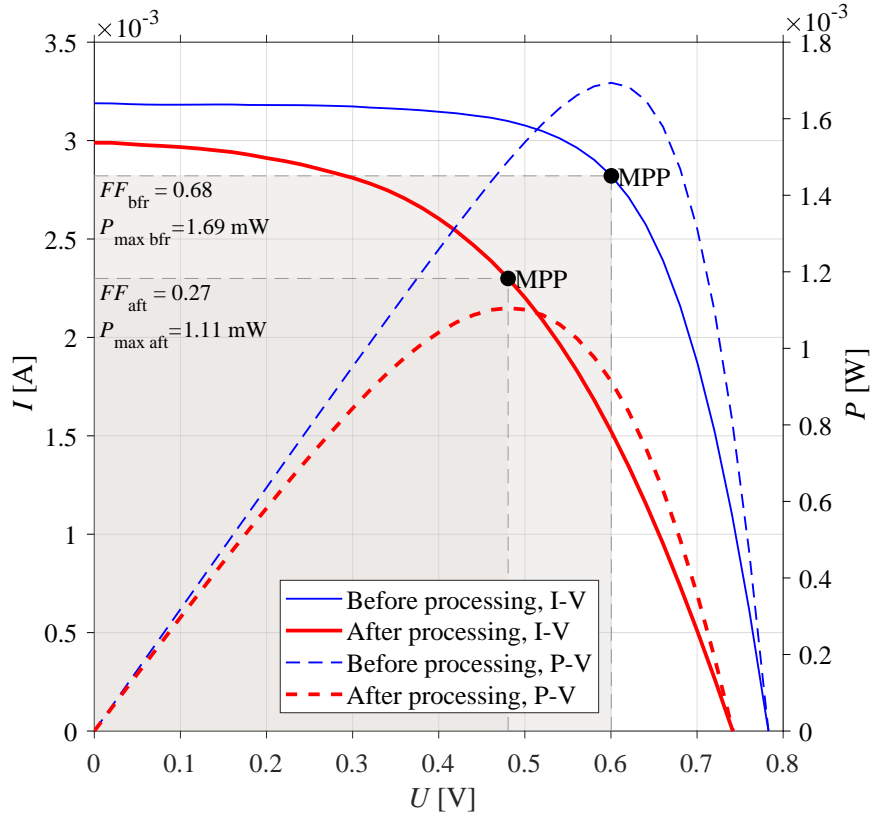


Figure 10: Current-voltage I-V and power P-V curves with ideal maximum power point before and after thermal processing.

3.7. Current noise power spectral density (PSD) investigation

Noise fluctuation measurements were indicated as the flicker noise which was described above in Section 2.7. The noise power is approximately inversely proportional to the frequency at whole spectrum. Along with increasing voltage, the noise spectra magnitude grew with almost identical slope of the PSD after thermal processing in Figure 11. The slope index was 1.27.

Solar cell noise grew by almost one order and at higher voltages changed the slope to $f^{-1.57}$ for the thermal treatment in Figure 12. It can be observed that, except for the voltage of 6 V, which is still in front of the knee of I-V reverse-biased curve, the noise at all remaining voltages shifted to a relatively

uniform level. There are much smaller noise spectra magnitude ranges contrary to the noise before processing [?].

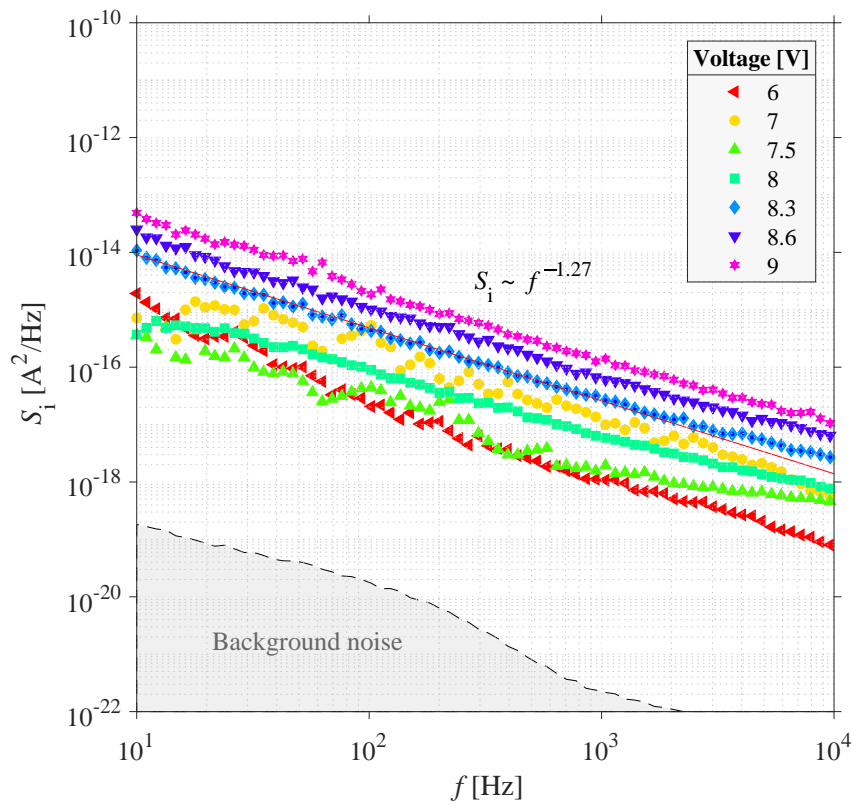


Figure 11: Flicker noise is visible on all measured voltages. Curves with a tension that extends behind the knee of the reverse-biased characteristic have a very similar character and the slope of index of 1.27.

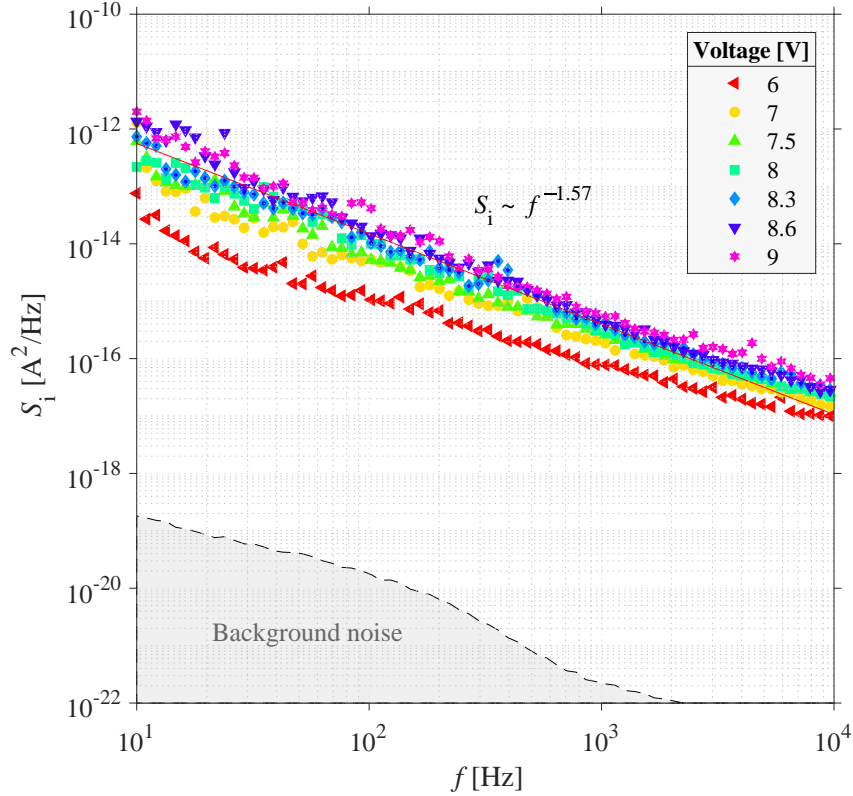


Figure 12: A smaller range and a higher noise spectra magnitude shift between the individual voltages and a greater slope with the index of 1.57 was observed after processing. This applies in particular to voltages above 7 V or higher.

3.8. Infrared camera investigation

245 Thermal radiation has appeared on several samples in other places than before after the thermal stress. Moreover, the radiated places existing before the processing were no longer present. It is obvious that while some of the defects ceased to exist, other appeared instead. This is confirmed by Figure 9 in the reverse bias, where the break on the curve after processing has changed.

250 Deformation of the defect or its disappearance durring treatment could lead to the different shape of break.

We also verified this by rotating and tilting the specimen and camera from

different angles to prevent camera reflection. This phenomenon can be seen in Figure 13, 14 and 15, where after processing the stressed parts have been created in other places. In order for these new defected parts to be visible, it was necessary to reduce the voltage from the original 7.3 V to 5 V. The influence of degradation was extensive so it could not be observed under the previous conditions.

The most of the other samples has already been manifested by the increasing intensity of radiation from the same area after thermal processing. This was the expected phenomena which we can attribute to the degradation of the cell [?].

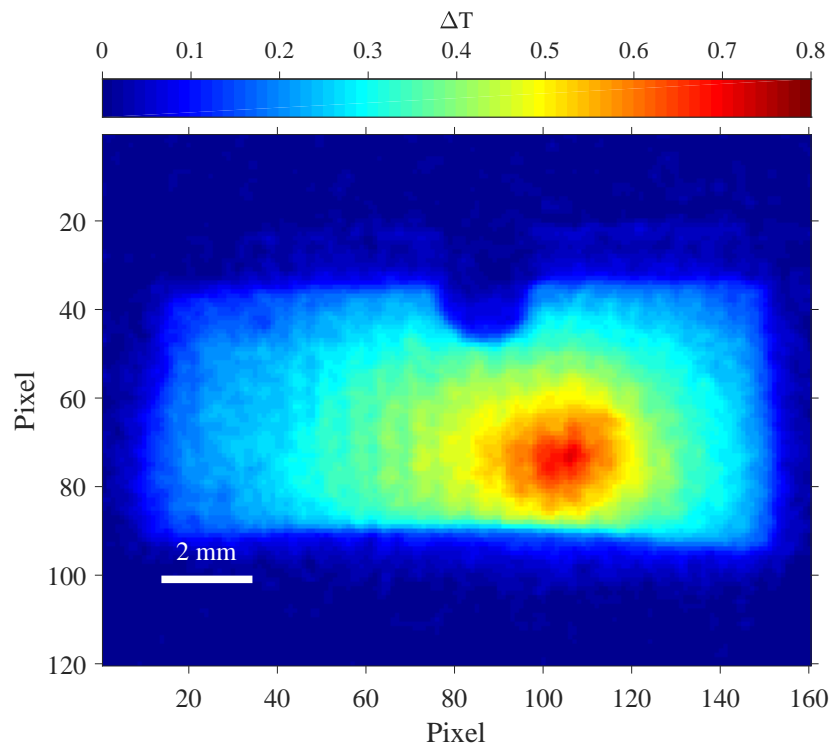


Figure 13: Photovoltaic cell under infrared camera at a voltage of 7.3 V before the thermal processing and its heat-generating location.

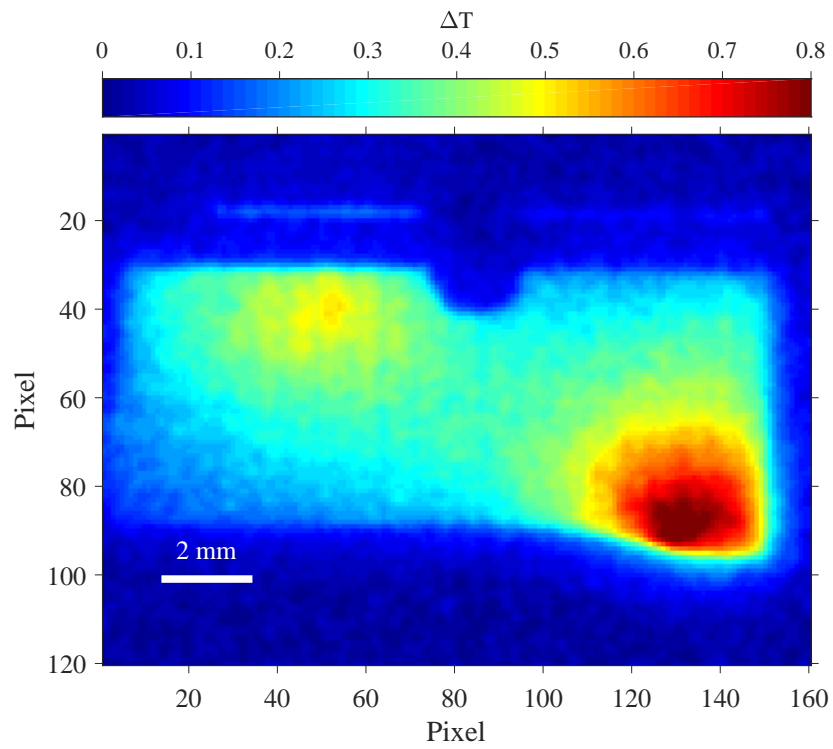


Figure 14: At several photovoltaic cells was occurred disappearance of the previous defects and other new defects creation after the thermal stress. On a given sample, it was necessary to reduce the voltage to 5 V due to its degradation and better localization of stressed places.

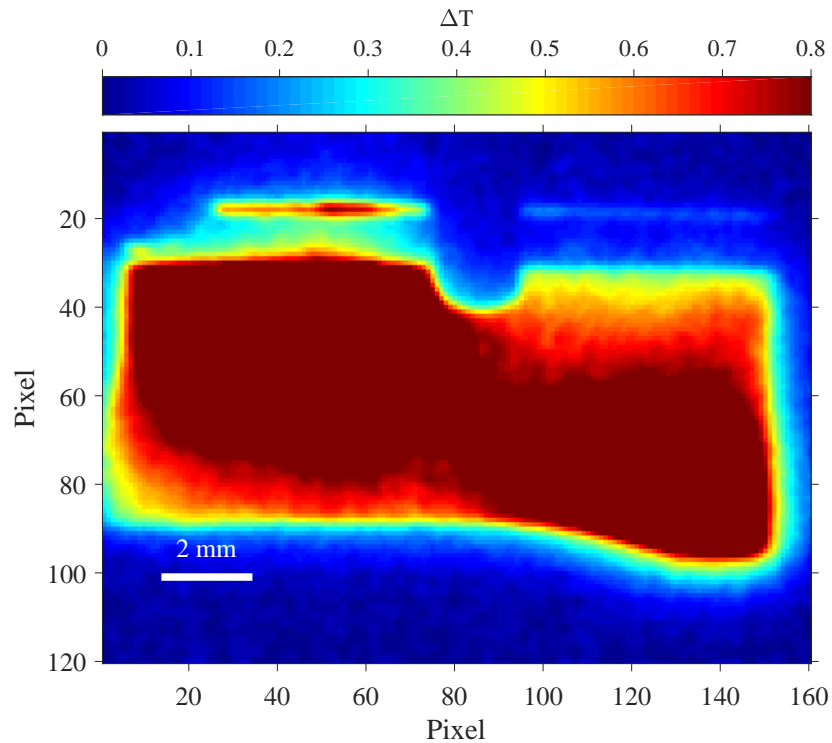


Figure 15: Photovoltaic cell under an infrared camera at 7.3 V after the thermal stress. At the same voltage, the difference compared to a cell before previous processing was very noticeable.

4. Conclusions

A comprehensive measurement of GaAs photovoltaic cells degradation has been performed. Surface morphology and electrical properties were studied. All evaluation methods were selected to complement each other. Each measurement provides different information and varies in data extraction. The results described above confirm the excellent stability of the material structure. In particular, the ratio of the elements remained almost unaltered after processing and their weight differences varied within a percentage of units. A slight oxidation of contacts has been observed but does not occur while used in space. However, the roughness of the surface and the number of structural features, which were examined using the atomic force microscope, increased slightly. The

thermal radiation of the cell in the case of reverse-bias has changed and increased. There were two undesirable phenomena. First was a difference in the
275 I-V characteristics, namely a decrease in its steepness. Second was a decrease
in cell power performance for P-V characteristics.

These results can be seen as very positive since the temperature range at
which the cells were thermally processed was at a relatively high level of 350 °C.
We observed the influence of temperature on the electric breakdown. A sudden
280 change occurs under reverse bias after increasing the processing temperature of
the solar cell to the limit of its functionality (420 °C). This change is in the form
of immediate electric breakdown. However, there are no significant changes in
the structure of the solar cell. Loss of functionality of the solar cell is mainly a
matter of internal phenomena.

285 **Acknowledgements**

Research described in the paper was financially supported by the Ministry of
Education, Youth and Sports of the Czech Republic under the project CEITEC
2020 (LQ1601), by the National Sustainability Program under grant LO1401,
by the Grant Agency of the Czech Republic under no. GACR 15-05259S and by
290 Internal Grant Agency of Brno University of Technology, grant No. FEKT-S-17-
4626. For the research, infrastructure of the SIX Center was used. Part of the
work was carried out with the support of CEITEC Nano Research Infrastructure
(MEYS CR, 2016–2019).